

Insights into the Growth of (Ultra)nanocrystalline Diamond by Combined Molecular Dynamics and Monte Carlo Simulations

Maxie Eckert,* Erik Neyts, and Annemie Bogaerts

Research group PLASMANT, Department of Chemistry, University of Antwerp Universiteitsplein 1, 2610 Antwerp, Belgium

Received January 18, 2010; Revised Manuscript Received May 7, 2010

ABSTRACT: In this paper, we present the results of combined molecular dynamics–Metropolis Monte Carlo (MD-MMC) simulations of hydrocarbon species at flat diamond (100)2 × 1 and (111)1 × 1 surfaces. The investigated species are considered to be the most important growth species for (ultra)nanocrystalline diamond ((U)NCD) growth. When applying the MMC algorithm to stuck species at monoradical sites, bonding changes are only seen for CH₂. The sequence of the bond breaking and formation as put forward by the MMC simulations mimics the insertion of CH₂ into a surface dimer as proposed in the standard growth model of diamond. For hydrocarbon species attached to two adjacent radical (“biradical”) sites, the MMC simulations give rise to significant changes in the bonding structure. For UNCD, the combinations of C₃ and C₃H₂, and C₃ and C₄H₂ (at diamond (100)2 × 1) and C and C₂H₂ (at diamond (111)1 × 1) are the most successful in nucleating new crystal layers. For NCD, the following combinations pursue the diamond structure the best: C₂H₂ and C₃H₂ (at diamond (100)2 × 1) and CH₂ and C₂H₂ (at diamond (111)1 × 1). The different behaviors of the hydrocarbon species at the two diamond surfaces are related to the different sterical hindrances at the diamond surfaces.

Introduction

Due to their outstanding chemical and physical properties, including chemical inertness,¹ high thermal conductivity,² and good biocompatibility,³ ultrananocrystalline and nanocrystalline diamond (UNCD and NCD) films have been studied intensively for the past decade.^{4–7} UNCD and NCD are grown by means of plasma-enhanced chemical vapor deposition (PE-CVD), either by microwave plasmas or by hot filament CVD.⁸ UNCD is a fine grain material with grain sizes between 3 and 5 nm, grown from a hydrogen poor plasma (typically 97% Ar/2% H₂/1% CH₄) and at relatively low substrate temperatures, typically 800 K.⁹ NCD consists of grains with diameter between 50 and 100 nm, and in contrast to UNCD, the grain size increases with the film thickness.⁹ Furthermore, NCD films are grown under conventional diamond PE-CVD conditions, that is, at higher substrate temperatures (≥1100 K) and from plasmas containing 1% CH₄ in H₂.⁹ In order to control the properties of the deposited (U)NCD films, which highly depend on the grain size, a detailed understanding of the growth mechanisms is required.

The detailed growth mechanisms of UNCD and NCD are still controversial¹⁰ and the subject of theoretical investigations.^{8,9} For CVD diamond, part of the growth is enlightened in the “standard growth mechanism”, which has been generally accepted since the early 1990s.¹¹ This model focuses on the growth at the diamond (100)2 × 1 surface, which is described by the addition of carbon atoms in an atom-by-atom mechanism. The added carbon atoms originate from CH₃, which is believed to be the main growth species,^{12–14} due to its high concentration above the surface.^{9,15} Until now, hydrocarbon species containing one carbon atom were supposed to be the only contributing species for diamond growth; because species with two or three carbon atoms can be removed from the surface through the

“β-scission” mechanism, they are not believed to contribute to the diamond growth.¹⁶ In the β-scission mechanism, a free electron of a stuck hydrocarbon species induces the break of a carbon–carbon bond that is two carbons away from the carbon atom with the free electron, resulting in a C_xH_y species that is released into the gas phase and a free electron at the surface. It is a fast, low energy reaction which is thought to prevent the formation of polymer chains at the surface and therefore to enhance the smoothness of the diamond surface.¹⁶

The carbon incorporation through CH₃ has been investigated extensively by means of computational methods, among which are classical molecular dynamics simulations,¹⁷ the density functional theory (DFT) method,^{18,19} hybrid quantum mechanical and molecular mechanics methods,^{20,21} and semi-empirical quantum–mechanical methods at the PM3 level.¹⁴ The reaction mechanism of CH₃ pursuing the diamond structure is described as follows:¹¹ First, the methyl radical (*CH₃) sticks to a dangling bond at the diamond surface (i.e., a surface radical *C_d generated by hydrogen abstraction): *C_d + *CH₃ → C_d–CH₃. In the next step, atomic hydrogen from the gas phase removes a hydrogen atom from the CH₃ group: C_d–CH₃ + *H → C_d–*CH₂ + H₂. This is followed by the opening of the surface dimer (H–C_d–C_d–*CH₂ → H–*C_d + C_d=CH₂). The two diamond surface atoms will be bridged by the (double-bonded) CH₂ group, forming a new carbon 6-ring and thus pursuing the diamond lattice. In the standard growth mechanism, atomic hydrogen from the gas phase, created by the dissociation of H₂, is the drive behind the chemistry of the diamond growth; by adsorbing hydrogen from the surface and from stuck radicals, atomic hydrogen creates reactive sites. Furthermore, atomic hydrogen can etch nondiamond phases back into the gas phase.²²

Besides the (100)2 × 1 surface, the (111)1 × 1 surface is also considered to be an important low-index diamond surface. However, the growth of CVD diamond at the (111)1 × 1 surface has not been studied at the same level of theory and as

*To whom correspondence should be addressed E-mail: maxie.eckert@ua.ac.be.

extensively as the growth at the diamond (100) 2×1 surface. Recently, Butler and Oleynik reported the formation of the next layer of growth at the diamond (111) 1×1 surface.¹³ The critical step of the formation of a new layer is as follows: An incoming CH₃ radical adsorbs at C_d-CH₂ (with the CH₂ group originating from C_d-CH₃ + *H → C_d-CH₂* + H₂; see above), forming C₂H₅: C_d-CH₂* + *CH₃ → C_d-CH₂-CH₃. If not desorbed through the β-scission reaction, C₂H₄ (generated by hydrogen abstraction from the C₂H₅ group) can form a three-atom bridging structure with a neighboring CH₂. In order to complete the island formation, another CH₂ at a neighboring diamond surface atom has to form a bond to the three-atom bridge structure.

For the growth of UNCD and NCD, the significance of the β-scission reaction has recently been doubted.¹⁰ May et al. investigated the effect of including the β-scission mechanism into a Monte Carlo (MC) model for the simulation of (U)NCD growth. They conclude that its importance in removing carbon atoms from the surface has been overestimated and that the β-scission reaction is rather unimportant for diamond growth. May et al. suggest that other hydrocarbons than the C₁H_y species might affect the growth rate of (U)NCD.⁸ Indeed, during the growth of (U)NCD, some C_xH_y species with $x \geq 2$ have higher concentrations than the C₁H_y species above the surface⁹ and have a high reactivity.²³ Investigating the behavior of those hydrocarbon species might therefore improve the standard growth model, regarding the discrepancy between the predictions of the model and the experimentally measured morphology and grain sizes of (U)NCD films.^{10,24}

Until now, the addition of CH₃ to *monoradical* sites at diamond surfaces, i.e., dangling bonds without neighboring dangling bonds, has been the main focus in theoretical investigations of diamond growth.^{11,13} For conventional diamond CVD conditions, the probability of two sites chosen at random both being radicals is as low as 0.01.¹⁴ Nevertheless, the addition of hydrocarbons to biradical sites might affect the growth of (U)NCD and, more general, the growth of CVD diamond: At biradical surface sites, two attached hydrocarbon species can cross-link, resulting in a renucleation point for a new epitaxial layer or for a new crystallite with a different orientation than the existing layer, affecting the growth of the film even when occurring only rarely.⁸

In the past, we investigated the behavior of various hydrocarbon species impacting diamond (100) 2×1 and (111) 1×1 surfaces.²³ By means of molecular dynamics (MD) simulations, we gained more insight on the atomic level into how hydrocarbon species contribute to the growth of (U)NCD, i.e., which C_xH_y species stick to diamond surfaces and contribute to hydrogen abstraction under typical conditions of (U)NCD growth. However, the time scale on which we can follow the evolution of the system by means of MD is limited to, at a maximum, the nanosecond time scale. Infrequent events, such as relaxational and diffusive events, are important for thin film growth.²⁵ They take place on the microsecond time scale, and therefore, they cannot be investigated by means of MD. To circumvent this “time-scale problem”, numerous computational techniques have been developed, such as the kinetic Monte Carlo (kMC) method.¹² Netto and Frenklach succeeded in developing a kMC method, which enables the fast simulation of diamond growth mimicking experimental results.¹² However, the applicability of the kMC method is restricted by the requirement that all relevant transitions and their rate constants have to be known in advance. Consequently, the reliability of kMC methods

strongly depends on the completeness of the catalogue containing the transition mechanisms. Unexpected diffusion behavior or new growth mechanisms cannot be discovered by means of kMC. An illustration of the caution that is necessary when selecting a certain kind of mechanism can be found in the literature.²⁶ Other techniques have been elaborated, such as the “accelerated dynamics methods” developed by the Los Alamos National Laboratory²⁶ and the activation–relaxation technique (ART).²⁷ In the ART, the system is first pushed up the energy path, followed by the relaxation into the adjacent energy minimum. In order to apply this technique properly, all relevant saddle points of the energy landscape need to be found, which limits the applicability of this method. The accelerated dynamics method with the greatest boost factor is called “temperature accelerated dynamics” (TAD).^{26,28} In essence, during a TAD simulation, the temperature of the system is raised such that infrequent events will be accelerated. The behavior of the system at the raised temperature is then extrapolated to the original (lower) temperature of the system. For a correct extrapolation, the transitions of the considered system need to obey the harmonic transition state theory,²⁸ which is not true for our systems at relatively high temperatures.

Therefore, we developed a new implementation of the Metropolis Monte Carlo (MMC) algorithm.²⁹ For the MMC algorithm, in its original form developed in the 1950s,³⁰ no transition mechanisms have to be known in advance, nor is the system temperature limited. We have shown that when coupled to an MD code, the integral evolution of impacting species during thin film growth can be followed.²⁹ This was also found by others.³¹ The MD part of the code allows the simulation of particle impacts, whereas the MMC part of the simulation accounts for the further slower evolution of adatoms at the growing surface.

In ref 29, the implementation of the MMC algorithm is verified by longer-time scale MD simulations: The MMC simulations and longer-time scale MD simulations lead to the same structures. However, the calculation time of the MMC simulations was typically 1 order of magnitude shorter than the MD calculation time.

In this paper, we present the results of a combined MD-MMC study that intends the discovery of which possible reactions various hydrocarbon species can undergo at growing diamond surfaces. The focus of this paper is to investigate the relaxational behavior of hydrocarbon species that are known to have a high reactivity at diamond surfaces²³ and a high concentration close to the surface during the growth of (U)NCD.⁹ Besides their behavior at monoradical sites, the behavior of couples of hydrocarbon species at biradical sites is studied in detail. It should be noted that although the method is here employed for the simulation of diamond growth, its applicability is not restricted to diamond growth.²⁹

Simulation Method

The term “combined molecular dynamics–Metropolis Monte Carlo simulation” (MD-MMC) refers to simulations for which the MD and MMC methods are alternated. One MD-MMC cycle follows one species impacting the surface by means of MD and the further evolution at the surface by the MMC method.

MC simulations are inherently different from MD simulations; in MC, the system evolves based on random numbers; that is, the simulations are probabilistic, whereas MD simulations

are deterministic. In MMC simulations, the system evolves by random displacements of its atoms or clusters of atoms. No activation barriers are taken into account, and the system evolves entirely based on its thermodynamic properties. Depending on the energy difference caused by the random move, this move is accepted or rejected. If the potential energy remains constant or decreases, the move is accepted. Otherwise, the move is accepted with a probability derived from Boltzmann's occupation probabilities for the states of a canonical ensemble. Thus, the MMC algorithm generates NVT ensembles based on the sampling of the Boltzmann distribution function.³⁰

An extensive description of the MD method can be found in ref 23. The MMC method as presented extensively in ref 29, has been improved, i.e., rotation of clusters of adatoms is now included. An outline of the MMC method and the description of the improvements that were carried out, is presented here.

In Figure 1, the flow chart of the present implementation of the coupled MD-MMC method can be found. It will be explained in detail in the following subsections. One MD-MMC cycle starts with the simulation of a C_xH_y species impacting a diamond surface. After the integration time of the MD simulation, typically 2.0 ps, the MMC part of the simulation is started.

In order to study the behavior of C_xH_y species on diamond (100) 2×1 and (111) 1×1 surfaces, which are the two most important diamond surfaces,³² we calculated the sticking and etch coefficients in a previous study.²³ Furthermore, May et al. calculated the concentrations of those species above the surface during the growth of UNCD and NCD.⁹ Based on those two investigations, we can predict which species have absolutely the most sticking events during the growth of UNCD and NCD. For UNCD, the product of concentration and sticking coefficient is the highest for C_2H_2 and C_3 ($\sim 10^{14} \text{ cm}^{-3}$), followed by C_3H_2 , C_4H_2 ($\sim 10^{13} \text{ cm}^{-3}$), C_2H , and C ($\sim 10^{12} \text{ cm}^{-3}$). For NCD, the product of concentration and sticking coefficient is the highest for C_2H_2 ($\sim 10^{13} \text{ cm}^{-3}$), followed by CH_3 and C_3H_2 ($\sim 10^{12} \text{ cm}^{-3}$). Hence, these species are investigated in the present study. As mentioned above, the behavior of the methyl radical at diamond (100) 2×1 has been the subject of study in large detail. As CH_2 (through hydrogen abstraction of CH_3) plays an important role during the mechanism of CH_3 insertion into a surface dimer,¹¹ CH_2 completes the list of hydrocarbon species of interest. In order to keep the measure of the list of hydrocarbon species reasonable, CH_2 is the only investigated species originating from hydrocarbon abstraction of another species.

Two types of surface reactions are studied: First, the behavior of those species is simulated at monoradical sites. Then, the behavior of *couples* of hydrocarbon species at biradical sites is looked at closely. The species that are investigated at the monoradical sites and at the biradical sites are listed in Table 1. In Figures 2 and 3, the arrangement of hydrocarbon species at the monoradical and biradical sites is illustrated for the diamond (100) 2×1 and (111) 1×1 surfaces. All simulations are carried out for diamond (100) 2×1 as well as for diamond (111) 1×1 . For each combination of impacting species at each of the two surfaces, 50 MMC simulations were carried out to have some statistically justified outcome.

Besides the different nature of the UNCD and NCD species (hydrogen poor and rich, respectively), the conditions for the simulation of the UNCD and NCD species at diamond surfaces differ by the system temperature. The UNCD species are investigated at a substrate temperature of 800 K and the NCD species at a substrate temperature of 1100 K. Therefore, in order to prepare the substrate for impacts of the UNCD

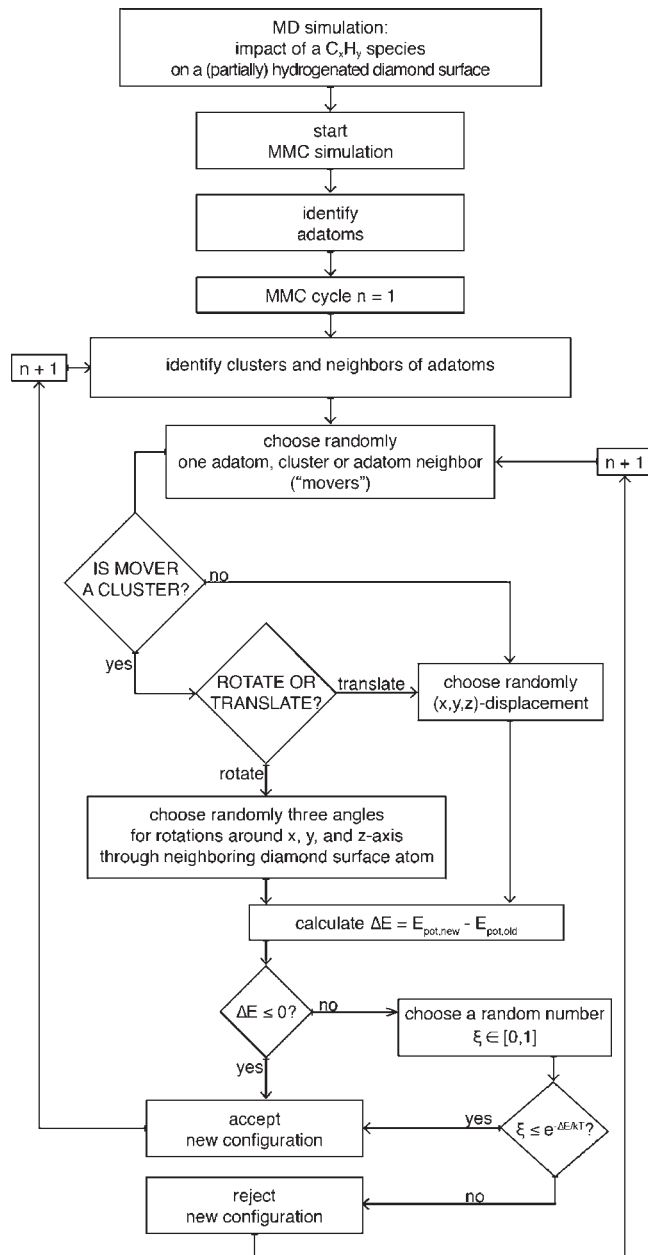


Figure 1. Flow chart of the MD-MMC simulation method applied for this paper. The MD part of the code simulates the impact of hydrocarbon species on a growing diamond surface, and the MMC part simulates the further evolution (see text).

and NCD species, the substrate is thermalized by the Berendsen heat bath to 800 K and 1100 K, respectively (a very detailed description of the thermalization can be found in ref 23). During the MD part of the simulation, no further heat bath is applied; that is, the system evolves freely. Furthermore, 800 and 1100 K are the system temperatures which are required for the MMC simulation (see below).

In the following, the combined MD-MMC model, as outlined in Figure 1, will be explained in more detail.

MD Simulation of Impacting C_xH_y . During the first part of the MD-MMC simulation, the impacts of the hydrocarbon species on partially hydrogenated diamond surfaces are carried out by means of MD. Classical molecular dynamics simulations have been used extensively in order to describe the interaction between impacting species and diamond surfaces.^{23,33–35} MD simulations take the dynamics of the

Table 1. Investigated Species Relevant for the Growth of UNCD (left part of the table) and NCD (right part of the table)^a

UNCD		NCD	
<i>monoradical sites</i>		<i>monoradical sites</i>	
C, C ₂ H, C ₂ H ₂ , C ₃ , C ₃ H ₂ , C ₄ H ₂		CH ₂ , CH ₃ , C ₂ H ₂ , C ₃ H ₂	
<i>biradical sites</i>		<i>biradical sites</i>	
C ₂ H ₂ next to one of	C, C ₂ H, C ₂ H ₂ , C ₃ , C ₃ H ₂ , C ₄ H ₂	C ₂ H ₂ next to one of	CH ₂ , CH ₃ , C ₂ H ₂ , C ₃ H ₂
C ₃ next to one of			

^aThe combinations of hydrocarbon species at biradical sites consist of (i) the hydrocarbon species with the most sticking events: [C₂H₂ or C₃ (for UNCD) and C₂H₂ (for NCD)] and (ii) a second hydrocarbon species with still a rather high number of sticking events (see text). For UNCD, this results in eleven combinations of hydrocarbon species, and for NCD, there are four combinations.

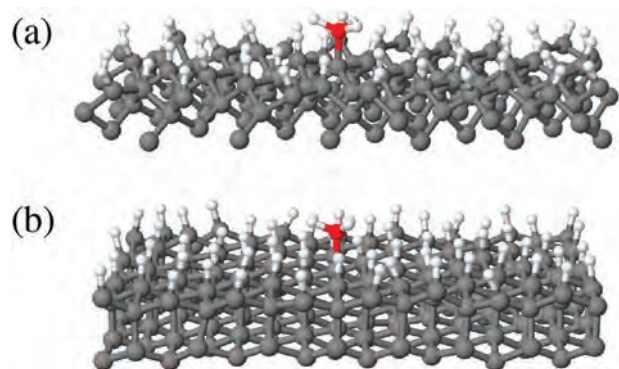


Figure 2. Hydrogenated diamond (100)2 × 1 (a) and diamond (111)1 × 1 (b) surfaces with a methyl radical attached to a monoradical site. The crystalline carbon atoms, the hydrogen atoms, and the carbon adatom are indicated by gray, white, and red spheres, respectively. For clarity reasons, only the four topmost atom layers are shown. The arrangement of other hydrocarbon species stuck to the monoradical sites of diamond (100)2 × 1 and diamond (111)1 × 1 is analogous to the structures shown in this figure, regarding the place of the stuck hydrocarbon species and bonds of the adatoms to the surface.

system into account: The atoms of the investigated system are followed through time and space based on Newtonian dynamics, interacting through a potential function.³⁶ For the growth of diamond structures, we apply the well-known Brenner potential, an empirical potential function for hydrocarbon structures.³⁷ In contrast to other empirical potential functions, this function describes well the structure of diamond surfaces, in agreement with quantum mechanical calculations.³⁸

In the Brenner potential function, the potential energy is expressed as a sum over bond energies between couples of atoms. The bond energies consist of repulsive and attractive components; their values depend on the scalar separation between the couples of atoms. Besides the attractive and repulsive terms, the “bond order” function determines the value of the bond energy. The bond order function models the many-body chemistry and accounts for the different behaviors of hydrogen and carbon.

In order to limit the interatomic potential range to first neighbors only, a so-called “cutoff function” is introduced. The range of the cutoff function is [0,1], and the components of the bond energy are multiplied by the function value. For interatomic distances smaller than the inner cutoff radius (i.e., 1.7 and 1.3 Å for C–C and C–H interactions, respectively), the value of the cutoff function equals 1, and therefore, the repulsive and attractive components are not affected. However, for interatomic distances greater than the outer cutoff radius (i.e., 2.0 and 1.8 Å for C–C and C–H interactions, respectively), the cutoff function equals 0 and no interaction between the atoms is taken into account. Between the inner and outer cutoff radii, the cutoff function value decays smoothly from 1 to 0. Furthermore, this cutoff function defines the bonding connectivity

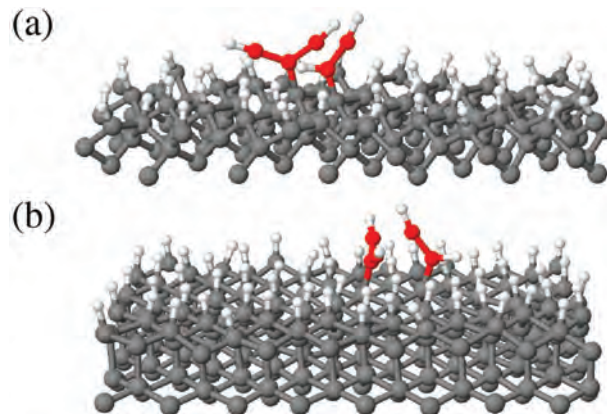


Figure 3. Hydrogenated diamond (100)2 × 1 (a) and diamond (111)1 × 1 (b) surfaces with C₂H₂ and C₃H₂ attached to a biradical site. The biradical site consists of two neighboring dangling bonds at the diamond surfaces; in the case of diamond (100)2 × 1, the dangling bonds are located within the same dimer row. The crystalline carbon atoms, the hydrogen atoms, and the carbon adatoms are indicated by gray, white, and red spheres, respectively. For clarity reasons, only the four topmost atom layers are shown. The arrangement of other hydrocarbon species stuck to the biradical sites of diamond (100)2 × 1 and diamond (111)1 × 1 is analogous to the structures shown in this figure, regarding the place of the stuck hydrocarbon species and bonds of the adatoms to the surface. For diamond (100)2 × 1, other configurations of biradical sites are also possible. Here, the biradical site consists of two dangling bonds at adjacent carbon atoms within one dimer row. In that case, the two carbon atoms with dangling bonds are connected through one other carbon atom, which is also true for the biradical site at diamond (111)1 × 1.

between the atoms of the system: The number of bonds in which a given atom is involved is calculated as the sum of the cutoff function values following from the scalar separations from the other atoms of the system. Other formulations of the cutoff are available, such as an environment-dependent first nearest-neighbor definition, which improves the reliability of simulations of pure carbon materials.³⁹

The substrates that will be impacted by the species relevant for UNCD and NCD growth have temperatures of 800 and 1100 K, respectively. For each of the two temperatures, two substrates have been constructed: diamond (100)2 × 1 and diamond (111)1 × 1. In this way, four different input configurations for the MD simulations can be distinguished.

Before the impacts, the partially hydrogenated diamond substrates contain 900 (diamond (100)2 × 1) and 768 (diamond (111)1 × 1) carbon atoms. In the case of the monoradical sites, the diamond (100)2 × 1 and (111)1 × 1 surfaces hold additionally 49 and 63 H atoms, respectively. One diamond surface atom is not passivated by a hydrogen atom (“dangling bond”, DB). Surfaces containing a biradical site hold one H atom less. The biradical site refers to two neighboring dangling bonds. For diamond (100)2 × 1, the

DB's are located at two neighboring surface dimers (along the dimer row). To prevent translation of the cell due to momentum transfer of impacting species, the lower two atomic layers (100 and 128 carbon atoms for diamond (100) and (111), respectively) are kept fixed. In the $\pm x$ and $\pm y$ direction (parallel to the surface), periodic boundary conditions are imposed. The construction of the diamond substrates is described extensively in ref 23.

In order to maximize the sticking probability, all simulated impacts are normal to the surface³⁵ and close to the dangling bond(s); the initial position of the impacting species in the $\{x,y\}$ -surface is randomly chosen within 1 \AA^2 of the dangling bond. For the biradical study, two successive impacts are carried out, in order to investigate the behavior of couples of hydrocarbon species under the influence of the MMC simulation. The impacting species are initially placed at a distance above the surface for which the interaction energy between the surface and the species is negligible. The species' translational, rotational, and vibrational energies correspond to a gas temperature of 2120 K.⁹ All impacts are followed for 2.0 ps. Once the MD simulation is finished (i.e., the integration time of 2.0 ps is reached), the output configuration is subject to the starting MMC simulation.

Definition of Movers and Trial Moves in MMC. After the integration time of 2.0 ps by the MD simulation, the MMC part of the model is started. The simulation starts with the decision of which atoms will be allowed to be displaced in the MMC simulation.

The number of atoms that are explicitly considered in the simulation of relaxational processes may be restricted to a certain atom type or subregion of the full system, preventing the simulation of events that might interfere with the processes that are the subject of the investigation, as stated by Kaukonen et al.⁴⁰ Since we are interested in adatom surface behavior, first of all, all adatoms, i.e., the atoms that do not belong to the crystalline phase, are identified. "Crystalline atoms" are atoms that, in the case of a growing diamond structure, are part of the diamond bulk; furthermore, all (hydrogen and carbon) atoms that are part of the (partially) hydrogenated diamond surface are classified as "crystalline". In ref 29, an extensive description of the identification of (non)crystalline atoms can be found. The adatoms remain classified as adatoms during the whole MMC simulation; that is, they will be allowed to be displaced and stored in the "movers list". At the beginning of each MMC cycle, the list of movers is completed: In order to take the local environment of the adatoms into account, analogous to other MC approaches,^{27,41,42} the neighbors of the adatoms are also identified as movers. In the list of movers, the adatoms are stored both individually and as clusters, in case adatoms are connected by chemical bonds ("clusters"). The clusters are stored *twice* in the list of movers, accounting for (i) displacement and (ii) rotation of the cluster. A very detailed justification of the selection of the movers can be found in ref 29. In order not to push the adatoms into a crystalline configuration, the adatoms will be allowed to be displaced during the whole MMC simulation; that is, the list of adatoms is not updated after every accepted trial move. In contrast to that, the changes of the local environment of the adatoms by the trial moves need to be taken into account, and therefore, the neighbors and clusters of adatoms are updated after every accepted move.

Once the list of movers is completed, one of the movers is chosen randomly. If the chosen mover is an atom, it will be translated by a randomly chosen (x,y,z) -displacement, a so-called "trial move". This trial position (x_n, y_n, z_n) is determined as follows from its original position (x_m, y_m, z_m) :³⁰

$$x_n \rightarrow x_m + \alpha(2\xi_1 - 1.0) \quad (1)$$

$$y_n \rightarrow y_m + \beta(2\xi_2 - 1.0) \quad (2)$$

$$z_n \rightarrow z_m + \gamma(2\xi_3 - 1.0) \quad (3)$$

ξ_i represents random numbers $\in [0,1]$. α , β , and γ represent the maximum displacements in the (x,y,z) -directions. Their values are chosen based on a criterion proposed by Frenkel et al.:³⁶ The optimum maximum displacements lead to the highest sum of squares of all accepted trial displacements per computing time. This criterion accounts for the lowest statistical error; the higher the sum of accepted trial displacements, the greater the distance covered in configuration space. For both the diamond (100) 2×1 and (111) 1×1 surfaces, the optimum value of α and β equals 2.8 \AA , whereas the value of γ equals 0.6 \AA and 0.8 \AA , respectively.²⁹ For the generation of random numbers, we applied a pseudorandom number generator, which uses a linear congruential algorithm and 48-bit integer arithmetic.

As mentioned above, the adatoms clusters are stored twice in the movers list, accounting for translation and rotation of the cluster. Only when a cluster is chosen from the movers list, does a random number decide whether the chosen cluster will be rotated or translated (with each a probability of 50%). If the cluster is translated, all adatoms that are part of the cluster are displaced according to formulas 1–3. In case the trial move is a rotation, the cluster is rotated about an arbitrary axis through the crystalline atom to which the cluster is bound, i.e., a diamond surface atom. In practice, the randomly chosen axis and the rotation angle are not applied explicitly but follow from successive rotations about the space-fixed z -, x -, and y -axes with the diamond surface atom at the origin. For the rotations about the axes, three random rotation angles, ϕ_x , ϕ_y , and $\phi_z \in [-\pi, \pi]$, are chosen. Note that this implementation does not result in completely uniform distributed rotation angles. The ergodicity is, however, still assured. The trial positions of the cluster's atoms are thus calculated by those three random rotation angles. The zxy -rotation matrix, denoting the successive rotation about the space-fixed z -, x -, and y -axes, is calculated as the product of three matrices, $\text{Rot}(y, \phi_y) \text{Rot}(x, \phi_x) \text{Rot}(z, \phi_z)$, giving the expression described by eq 4.

In the previous implementation of the MMC algorithm, no cluster rotation was included.²⁹ Here, we compare results obtained with and without the cluster rotation for the same input configurations. The calculation data for three examples are summarized in Table 2.

During the MMC simulation of C and C_2H_2 at diamond (111) 1×1 and C_3 at diamond (100) 2×1 , there are a few accepted trial rotations among the MMC cycles. As can be concluded from the table, the number of MMC cycles needed to reach convergence (see below), is reduced significantly.

$$zxy = \begin{bmatrix} \cos(\phi_y) \cos(\phi_z) + \sin(\phi_x) \sin(\phi_y) \sin(\phi_z) & \cos(\phi_z) \sin(\phi_x) \sin(\phi_y) - \cos(\phi_y) \sin(\phi_z) & \cos(\phi_x) \sin(\phi_y) \\ \cos(\phi_x) \sin(\phi_z) & \cos(\phi_x) \cos(\phi_z) & -\sin(\phi_x) \\ \cos(\phi_y) \sin(\phi_x) \sin(\phi_z) - \cos(\phi_z) \sin(\phi_y) & \cos(\phi_y) \cos(\phi_z) \sin(\phi_x) + \sin(\phi_y) \sin(\phi_z) & \cos(\phi_x) \cos(\phi_y) \end{bmatrix} \quad (4)$$

Table 2. Comparison of the Calculation Data of the Previous Implementation without Cluster Rotation (Presented in Ref 29) and the Improved Model Including Cluster Rotation as Employed for This Paper^a

		cluster rotation <i>not</i> implemented	cluster rotation implemented
C and C ₂ H ₂ at (111)1 × 1	<i>t</i> _{calc} (min)	356	93
	number of MMC cycles	391 046	74 332
	number of MMC cycles/min	1098	799
	number of accepted moves	47	27
	number of accepted rotations		1
C and C ₄ H ₂ at (111)1 × 1	<i>t</i> _{calc} (min)	20	27
	number of MMC cycles	21 688	21 498
	number of MMC cycles/min	1084	796
	number of accepted moves	17	14
	number of accepted rotations		0
C ₃ at (100)2 × 1	<i>t</i> _{calc} (min)	252	173
	number of MMC cycles	301 893	158 798
	number of MMC cycles/min	1197	918
	number of accepted moves	27	29
	number of accepted rotations		2

^a *t*_{calc} refers to the total calculation time of the MMC simulation, and number of MMC cycles to the number of cycles needed to reach convergence.

This can be understood by the fact that a rotation can be interpreted as a grouped displacement that corresponds to a lot of separate trial displacements of each member of the rotator. Despite a higher average calculation time per MMC cycle (due to the trigonometric functions), the calculation time decreases as well. However, for the case of C and C₄H₂ at diamond (111)1 × 1, no trial rotation is accepted, as can be seen in Table 2, and the number of MMC cycles does not decrease remarkably. Therefore, in this case, the calculation time increases slightly.

The decrease of the calculation time due to accepted rotations equals 74% (C and C₂H₂ at diamond (111)1 × 1) and 31% (C₃ at diamond (100)2 × 1), whereas the calculation time is raised by 35% in the case where no rotation is accepted (C and C₄H₂ at diamond (111)1 × 1). Nevertheless, the increase of the calculation time for a comparable number of MMC cycles in this last case does not compensate for the benefit of the implementation of rotation for the other cases, i.e., a decrease of the calculation time due to the sharp decrease of the number of MMC steps that need to be carried out.

Calculation of the Transition Probability in MMC. Once the trial configuration is found, the energy difference between the original configuration *m* and the trial configuration *n*, $\Delta E_{m \rightarrow n} = E_n - E_m$, is calculated. If the energy decreases by the trial move or remains constant, the trial configuration is accepted. In the case where the energy increases, the transition probability is calculated, applying the Boltzmann distribution function for the occupation probability *P_i* for a state *i* of a canonical ensemble at temperature *T*:⁴³

$$P_i = \frac{1}{Z} e^{-E_i/k_B T}, \text{ with the partition function} \\ Z = \sum_j e^{-E_j/k_B T} \quad (5)$$

Here, *E_i* and *k_B* represent the energy of state *i* and the Boltzmann constant. The probability of the transition from a lower energy to a higher energy state with energy difference $\Delta E_{m \rightarrow n}$ is then calculated by the ratio of the occupation probabilities, resulting in $P_{m \rightarrow n} = e^{-\Delta E_{m \rightarrow n}/k_B T}$.³⁰ A random number then decides whether the transition to the higher energy state is accepted: In case the random number is greater than $P_{m \rightarrow n}$, the transition $m \rightarrow n$ is rejected; otherwise, it is accepted.

Concluding the MMC Simulation. The sequence of choosing trial moves and following acceptance or rejection of

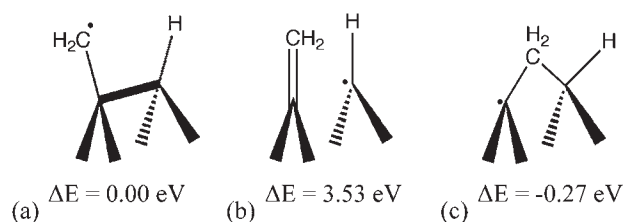


Figure 4. CH₂ stuck to a monoradical site at diamond (100)2 × 1 (a), further evolution (b), and final configuration (c). The energy differences with respect to the configuration shown in part a are also given and calculated as follows: The potential energy of the configurations that do not exhibit bond changes when minimized by the MMC simulation is set to 0.0 eV; other energies are expressed with respect to that value. All energy differences presented in this paper are calculated in this manner.

these trial moves is repeated until the energy of the system is “converged” and no new trial moves are accepted. The following convergence criterion is implemented:²⁹ The simulation is finished, as soon as the number of adjacent rejected moves equals half the number of all trial moves that have been carried out. It has been shown that this criterion is strict enough.²⁹ Depending on the energetics of the starting configuration, it takes 10⁴–10⁵ cycles to reach convergence.²⁹

Results and Discussion

After the MD simulation, the stuck hydrocarbons have one bond with the surface (see Figures 2 and 3). This is the most probable configuration at substrate temperatures between 800 and 1100 K.²³ In this section, the resulting configurations after the MMC simulations will be discussed, first for the monoradical sites, and subsequently for the biradical sites. Furthermore, the effect of the system temperature (eq 5) has been investigated, as discussed below.

Monoradical Sites. In the case of UNCD growth, there are no bond changes observed during the MMC simulations of the relevant hydrocarbon growth species attached to monoradical sites at both diamond surfaces. For NCD growth, there is only one case for which bond changes are seen in the resulting structures of the MMC simulations, i.e., CH₂ inserting into the surface dimer at diamond (100)2 × 1. Nevertheless, this bond change is only observed *once* for all 50 MMC simulations that have been carried out.

In Figure 4, the evolution and energetics of the CH_2 inserting into the surface dimer is shown. Note that the sequence a–c in Figure 4 follows exactly the reaction mechanism of CH_2 insertion into a surface dimer as proposed in the standard growth model (see Introduction). Furthermore, the energy difference between the starting (Figure 4a) and end configurations (Figure 4c, -0.27 eV) corresponds remarkably well to reported values in the literature. Indeed, in refs 20 and 21, it is reported that the energy difference between the adsorbed CH_2 at the dimer and the ring closing steps calculated by quantum mechanical approaches varies between -0.015 and -0.522 eV. Furthermore, the energy decrease due to the insertion of CH_2 approaches well the value Garrison et al. report (i.e., -0.20 eV) when applying the same interaction potential function during a MD simulation.¹⁷ However, the potential energy after the dimer opening in our simulation (Figure 4b, 3.53 eV) is much higher than the reported values for this configuration from the literature (-0.022 to 0.856 eV).^{17,19,20} This is not surprising, since, in our method, no energy optimization after the dimer opening has been carried out in order to obtain a correct value of the potential energy.

Furthermore, from our MMC simulations, we can conclude that CH_2 (generated by hydrogen abstraction from CH_3) is the only species that contributes to diamond growth when attached to a monoradical site. This confirms the standard growth model. In addition, it justifies the investigation of hydrocarbon species at diamond surfaces by means of the coupled MD-MMC method. For the other species than CH_2 , the resulting configurations from the MD simulations of the sticking event, i.e., with one bond to the surface, determine the final bonding configuration, regardless of whether MMC is applied or not. Therefore, it is conceivable that if an impacting hydrocarbon species sticks to a dangling bond next to a previously stuck hydrocarbon species, the first hydrocarbon species still has one bond with the surface, regardless of the time between the two impacts. The behavior of those configurations will be discussed below, that is, the results for the cases of two hydrocarbon species stuck to two adjacent radical sites (so-called “biradical sites”).

Biradical Sites. In contrast to the MMC simulations for the monoradical sites, in the case of biradical sites, the MMC simulations give rise to significant changes in the configuration. In Tables 3–6, the resulting configurations obtained by the MMC simulations for biradical sites are shown, together with the corresponding probabilities. The results will be explained below for the different cases that were investigated, first for UNCD growth, and subsequently for NCD growth.

Here, it needs to be realized that the formation of new carbon 6-rings pursues the existing diamond structure. Three carbon atoms on a flat surface, together with three atoms of the existing diamond lattice, can form a carbon 6-ring. This means that the nucleus of a new diamond layer is formed, which is referred to as the “carbon 6-ring” in this paper. That is, here, we focus on the initial stage of growth, which is the formation of new islands. Those islands can, at a later stage of growth, evolve into terraces.

Species Important for UNCD Growth. As mentioned above, for UNCD, C_2H_2 , and C_3 are the hydrocarbon species with the most frequent sticking events. Hence, the behavior of these species in combination with the other important growth species for UNCD, as was outlined in Table 1 above, will be investigated. As shown in, for example, Table 3, C_2H_2

stuck at the surface contains at least one free electron at the carbon atom that is the farthest from the diamond surface. C_3 contains at least three free electrons, and the most probable configuration has one electron pair at the carbon atom the farthest from the surface and one free electron at the carbon atom the closest to the diamond surface (see e.g. Table 3).

The formation of carbon 6-rings by the combinations of species important for UNCD growth (see Table 1) is presented in Tables 3 and 4 for the two different diamond surfaces and can be summarized as follows.

- (i) In the case of the combinations with C_3 , the C atom closest to the surface (with its free electron) forms a bond to the other hydrocarbon species at the neighboring surface dimer. There are the following exceptions:
 - The combination with C, where the middle C-atom of C_3 binds to C, forming a 6-ring; alternatively, when the C-atom of C_3 closest to the surface binds to C, a carbon 5-ring would be formed, which seems in this case more probable.
 - The combination of C_3 and C_3 : In the case of diamond $(100)2 \times 1$, no carbon 6-rings are formed; in the case of diamond $(111)1 \times 1$, only one of the two C_3 can form a bond by its C atom closest to the surface in order to form a carbon 6-ring.
 - The combination of C_3 with C_2H at diamond $(100)2 \times 1$: No carbon 6-rings are formed.
- (ii) In the case of the combinations with C_2H_2 , the C atom the farthest from the surface (with its free electron) binds to the C atom of the other species closest to the surface. There are two exceptions: For the combination of C_2H_2 and C_3H_2 , the carbon 6-ring is formed by the C atom of C_3H_2 farthest from the surface, since there is too much sterical hindrance at the other carbon atom; on the other hand, for the combination of twice C_2H_2 , no carbon 6-ring is formed.

The formation of the other possible configurations (different from the 6-rings) is summarized briefly as follows (see again Tables 3 and 4): For the combinations with C_3 at both diamond surfaces and the combinations of C_2H_2 at diamond $(100)2 \times 1$, other ring structures are formed, in the majority of the cases by the carbon atoms of the hydrocarbon species the farthest from the surface. At the diamond $(111)1 \times 1$ surface, C_2H_2 is dehydrogenated without the formation of new C–C bonds, such that C_2H and C_xH_{y+1} is formed.

From Tables 3 and 4, it can be deduced which combinations of species at biradical sites have the highest probability to form carbon 6-rings and, hence, contribute effectively to diamond growth. At diamond $(100)2 \times 1$ (shown in Table 3), the highest probability to pursue the diamond structure is seen for the combination of C_3 and C_3H_2 (probability of 6-ring formation = 0.86), and C_3 and C_4H_2 (probability of 6-ring formation = 0.82). At diamond $(111)1 \times 1$, however, those combinations are much less successful in forming carbon 6-rings: The combinations of C_3 and C_3H_2 and C_3 and C_4H_2 have a probability of only 0.28 and 0.20, respectively, to form carbon 6-rings, as can be seen from Table 4. The most important combination for diamond growth at the $(111)1 \times 1$ surface is C and C_2H_2 (probability of 6-ring formation = 0.84). On the other hand, at diamond $(100)2 \times 1$, this combination leads to carbon 6-rings at a probability of only 0.04.

Table 3. Overview of the Mechanisms Occurring for the Hydrocarbon Species Important for UNCD Growth at a Biradical Site of Diamond (100)2 × 1^a

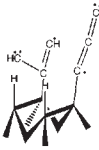
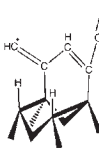
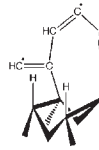
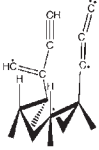
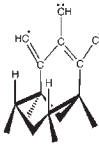
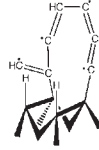

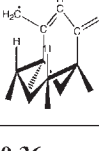
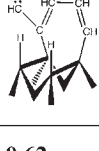
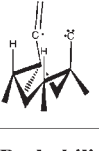
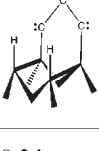

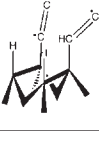
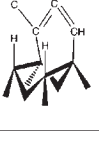
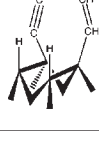
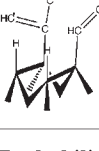


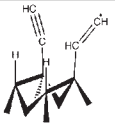
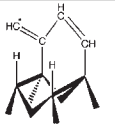
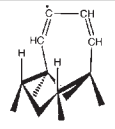
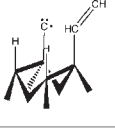
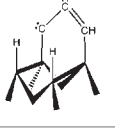
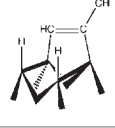
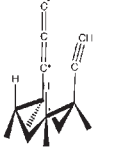
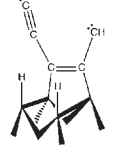
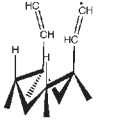
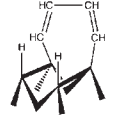
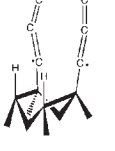
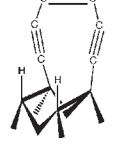
input configuration at diamond (100)2x1	resulting configuration		
	new carbon 6-ring	no new C–H or C–C bonds	other
C ₃ and C ₃ H ₂ 			
Probability $\Delta E =$	0.86 -5.47 eV	0.12 0.00 eV	0.02 -4.48 eV
C ₃ and C ₄ H ₂ 			
Probability $\Delta E =$	0.82 -5.29 eV	0.02 0.00 eV	0.16 -4.38 eV
C ₂ H ₂ and C ₃ H ₂ 			
Probability $\Delta E =$	0.36 -5.10 eV	0.02 0.00 eV	0.62 -4.00 eV
C ₃ and C 			
Probability $\Delta E =$	0.24 -2.97 eV	0.02 0.00 eV	0.74 -3.83 eV
C ₃ and C ₂ H ₂ 			
Probability $\Delta E =$	0.16 -3.78 eV	0.06 0.00 eV	0.78 -2.98 eV
C ₂ H ₂ and C ₄ H ₂ 			
Probability $\Delta E =$	0.10 -3.67 eV	0.02 0.00 eV	0.88 -3.80 eV

Table 3. Continued

input configuration at diamond (100)2x1	resulting configuration		
	new carbon 6-ring	no new C–H or C–C bonds	other
C_2H_2 and C_2H 			
Probability $\Delta E =$	0.06 -1.00 eV	0.88 0.00 eV	0.06 -0.76 eV
C_2H_2 and C 			
Probability $\Delta E =$	0.04 -5.02 eV	0.02 0.00 eV	0.94 -3.81 eV
C_3 and C_2H 			
Probability $\Delta E =$	0.00	0.94 0.00 eV	0.06 -2.19 eV
C_2H_2 and C_2H_2 			
Probability $\Delta E =$	0.00	0.02 0.00 eV	0.98 -4.75 eV
C_3 and C_3 			
Probability $\Delta E =$	0.00	0.02 0.00 eV	0.98 -6.13 eV

^a In the left column, the input configuration is shown. In the other columns, the resulting configurations calculated from 50 MMC simulations are shown: In the middle column, the configuration of the carbon 6-ring, which is the essential step in the diamond growth, is shown, together with its probability and energy decrease due to the configuration change. The energy decrease is calculated as the average energy decrease for the identical resulting configurations (the calculated standard error is smaller than 0.01). Identical structures are defined as structures with the same arrangement of chemical bonds. In the right column, the most probable of the other resulting configurations with changed C–C bonds is displayed together with the probability of a C–C bond change different from the formation of carbon 6-rings. The corresponding energy is the weighted average of the other configurations with changed C–C bonds. Furthermore, the probability for energy minimization without the formation of new C–C or C–H bonds is given. Probabilities are calculated as relative occurrences of the given structures after the MMC simulation. The combinations are sorted from top to bottom by decreasing probability of carbon 6-ring formation.

Despite the fact that the empirical Brenner potential will not calculate the energies at the same level of theory as, for example, DFT, the Brenner energies serve as a good indication for the energetics. Tables 3 and 4 show that those

differences cannot be elucidated exclusively by the energetics of the starting and end configurations: For, for example, C and C_2H_2 , the formation of a carbon 6-ring results in a decrease of the potential energy by 5.02 eV (diamond

Table 4. Overview of the Mechanisms Occurring for the Hydrocarbon Species Important for UNCD Growth at a Biradical Site of Diamond (111)1 × 1^a

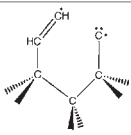
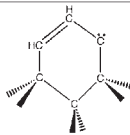
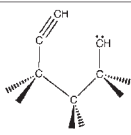
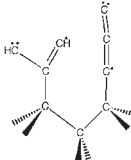
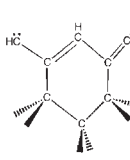
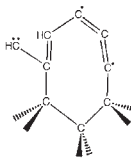
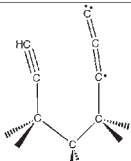
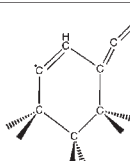
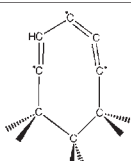
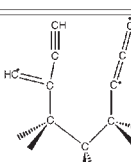
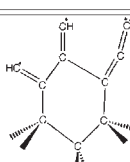
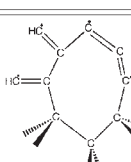
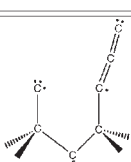
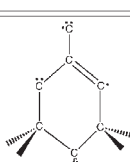
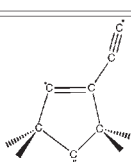
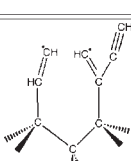
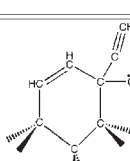
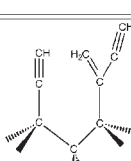
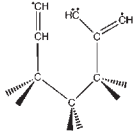
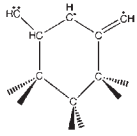
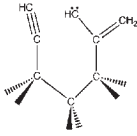
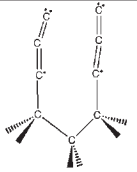
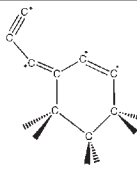
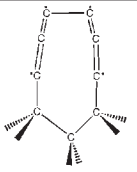
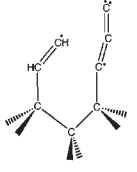
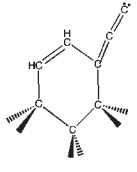
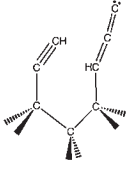
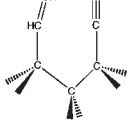
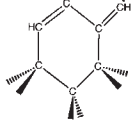
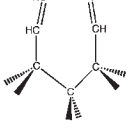
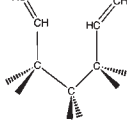
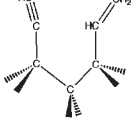
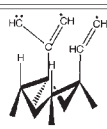
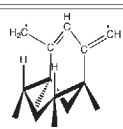
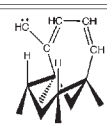
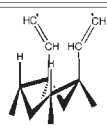
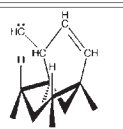
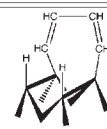
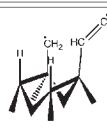
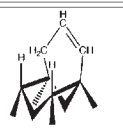
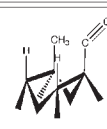
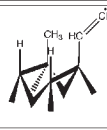
input configuration at diamond (111)1x1	resulting configuration		
	new carbon 6-ring	no new C–H or C–C bonds	other
C ₂ H ₂ and C 			
Probability ΔE =	0.84 -5.43 eV	0.02 0.00 eV	0.14 -3.50 eV
C ₃ and C ₃ H ₂ 			
Probability ΔE =	0.28 -5.02 eV	0.02 0.00 eV	0.70 -5.18 eV
C ₃ and C ₂ H 			
Probability ΔE =	0.20 -2.19 eV	0.38 0.00 eV	0.42 -1.96 eV
C ₃ and C ₄ H ₂ 			
Probability ΔE =	0.20 -4.63 eV	0.02 0.00 eV	0.78 -4.27 eV
C ₃ and C 			
Probability ΔE =	0.18 -2.28 eV	0.02 0.00 eV	0.80 -3.14 eV
C ₂ H ₂ and C ₄ H ₂ 			

Table 4. Continued

input configuration at diamond (111)1x1	resulting configuration		
	new carbon 6-ring	no new C–H or C–C bonds	other
Probability $\Delta E =$	0.14 -6.79 eV	0.02 0.00 eV	0.84 -5.40 eV
C_2H_2 and C_3H_2 			
Probability $\Delta E =$	0.10 -5.95 eV	0.02 0.00 eV	0.88 -4.48 eV
C_3 and C_3 			
Probability $\Delta E =$	0.08 -4.20 eV	0.02 0.00 eV	0.90 -5.79 eV
C_2H_2 and C_3 			
Probability $\Delta E =$	0.06 -4.73 eV	0.02 0.00 eV	0.92 -3.13 eV
C_2H_2 and C_2H 			
Probability $\Delta E =$	0.04 -1.47 eV	0.94 0.00 eV	0.02 -1.71 eV
C_2H_2 and C_2H_2 			
Probability $\Delta E =$	0.00	0.02 0.00 eV	0.98 -3.46 eV

^aIn the left column, the input configuration is shown. In the other columns, the resulting configurations calculated from 50 MMC simulations are shown: In the middle column, the configuration of the carbon 6-ring, which is the essential step in the diamond growth, is shown, together with its probability and energy decrease due to the configuration change. The energy decrease is calculated as the average energy decrease for the identical resulting configurations (the calculated standard error is smaller than 0.01). Identical structures are defined as structures with the same arrangement of chemical bonds. In the right column, the most probable of the other resulting configurations with changed C–C bonds is displayed together with the probability of a C–C bond change different from the formation of carbon 6-rings. The corresponding energy is the weighted average of the other configurations with changed C–C bonds. Furthermore, the probability for energy minimization without the formation of new C–C or C–H bonds is given. Probabilities are calculated as relative occurrences of the given structures after the MMC simulation. The combinations are sorted from top to bottom by decreasing probability of carbon 6-ring formation.

Table 5. Overview of the Mechanisms Occurring for the Hydrocarbon Species Important for NCD Growth at a Biradical Site of Diamond $(100)2 \times 1^a$

input configuration at diamond $(100)2 \times 1$	resulting configuration		
	new carbon 6-ring	no new C–H or C–C bonds	other
C_2H_2 and C_3H_2 			
Probability $\Delta E =$	0.28 -5.17 eV	0.02 0.00 eV	0.70 -4.58 eV
C_2H_2 and C_2H_2 			
Probability $\Delta E =$	0.16 -2.89 eV	0.02 0.00 eV	0.82 -3.82 eV
C_2H_2 and CH_2 			
Probability $\Delta E =$	0.08 -4.18 eV	0.02 0.00 eV	0.90 -2.37 eV
C_2H_2 and CH_3 			
Probability $\Delta E =$	0.00	1.00 0.00 eV	0.00

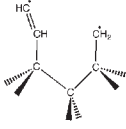
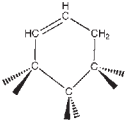
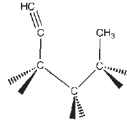
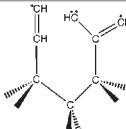
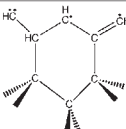
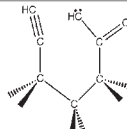
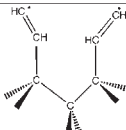
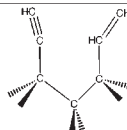
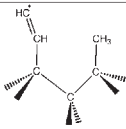
^a In the left column, the input configuration is shown. In the other columns, the resulting configurations calculated from 50 MMC simulations are shown: In the middle column, the configuration of the carbon 6-ring, which is the essential step in the diamond growth, is shown, together with its probability and energy decrease due to the configuration change. The energy decrease is calculated as the average energy decrease for the identical resulting configurations (the calculated standard error is smaller than 0.01). Identical structures are defined as structures with the same arrangement of chemical bonds. In the right column, the most probable of the other resulting configurations with changed C–C bonds is displayed together with the probability of a C–C bond change different from the formation of carbon 6-rings. The corresponding energy is the weighted average of the other configurations with changed C–C bonds. Furthermore, the probability for energy minimization without the formation of new C–C or C–H bonds is given. Probabilities are calculated as relative occurrences of the given structures after the MMC simulation. The combinations are sorted from top to bottom by decreasing probability of carbon 6-ring formation.

$(100)2 \times 1$) and by 5.43 eV (diamond $(111)1 \times 1$). The other resulting configurations lead to an average energy decrease of 3.81 and 3.50 eV, respectively. Hence, for both diamond surfaces, the energy drops as the configuration changes, and the energy decrease for the two diamond surfaces differs only by 0.3–0.4 eV, which is not reflected by similar probabilities of formation. More generally, as the probability of 6-ring formation decreases (downward the tables), no clear trend regarding the energetics can be observed. In other words, the energetics of the formation of the carbon 6-rings and other structures do not imply which resulting structure is favored. Therefore, it seems that it is not the minimum energy configuration that determines the resulting structure but the configuration space during the MMC simulation. Due to the surface structure, trial rotations will experience a certain sterical hindrance, which lowers the entropy of the

structure. This implies that the free-energy is lower for the configuration before the trial rotation and, hence, that the system is more probable to remain in the configuration space of the minimum energy configuration than evolving into the minimum energy configuration.

In Figure 5, the environment of a hydrocarbon species at diamond $(100)2 \times 1$ and $(111)1 \times 1$ is shown. As can be seen, at diamond $(100)2 \times 1$, the reconstruction leads to a surface structure in which a so-called “trough”⁴⁴ is formed between the surface dimers. Therefore, during the MMC simulation, a hydrocarbon species attached to a surface dimer at diamond $(100)2 \times 1$ will encounter less sterical hindrance than one at diamond $(111)1 \times 1$, enhancing the acceptance of trial rotations at diamond $(100)2 \times 1$. Therefore, it can be expected that, for hydrocarbon species with three or more carbon atoms, the minimum energy configuration is more

Table 6. Overview of the Mechanisms Occurring for the Hydrocarbon Species Important for NCD Growth at a Biradical Site of Diamond (111)1 × 1^a

input configuration at diamond (111)1 × 1	resulting configuration		
	new carbon 6-ring	no new C–H or C–C bonds	other
C_2H_2 and CH_2 			
Probability $\Delta E =$	0.30 -4.88 eV	0.04 0.00 eV	0.66 -3.11 eV
C_2H_2 and C_3H_2 			
Probability $\Delta E =$	0.18 -5.80 eV	0.02 0.00 eV	0.80 -4.72 eV
C_2H_2 and C_2H_2 			
Probability $\Delta E =$	0.00	0.04 0.00 eV	0.96 -3.22 eV
C_2H_2 and CH_3 			
Probability $\Delta E =$	0.00	1.00 0.00 eV	0.00

^aIn the left column, the input configuration is shown. In the other columns, the resulting configurations calculated from 50 MMC simulations are shown: In the middle column, the configuration of the carbon 6-ring, which is the essential step in the diamond growth, is shown, together with its probability and energy decrease due to the configuration change. The energy decrease is calculated as the average energy decrease for the identical resulting configurations (the calculated standard error is smaller than 0.01). Identical structures are defined as structures with the same arrangement of chemical bonds. In the right column, the most probable of the other resulting configurations with changed C–C bonds is displayed together with the probability of a C–C bond change different from the formation of carbon 6-rings. The corresponding energy is the weighted average of the other configurations with changed C–C bonds. Furthermore, the probability for energy minimization without the formation of new C–C or C–H bonds is given. Probabilities are calculated as relative occurrences of the given structures after the MMC simulation. The combinations are sorted from top to bottom by decreasing probability of carbon 6-ring formation.

frequently reached for the case of diamond (100)2 × 1, resulting in a higher probability of configurations containing the lowest potential energy (i.e., the carbon 6-ring).

As the rotation of C_3H_2 experiences less sterical hindrance at diamond (100)2 × 1 than at diamond (111)1 × 1, the probability that a trial rotation about an arbitrary axis is accepted is higher for diamond (100)2 × 1. At diamond (100)2 × 1, it is likely that the carbon atom the farthest from the surface is displaced into the trough (either by rotation or translation), as illustrated in Figure 5. This move into the trough will lower the sterical hindrance at the carbon atom bound to the diamond surface, promoting the formation of bonds between that atom and the neighboring stuck hydrocarbon species (i.e., enhancing the formation of 6-rings; see Table 3). In contrast to that, C_3H_2 is, due to the sterical

hindrance, forced to stand upright at the diamond (111)1 × 1 surface (see Figure 5), promoting the probability of bond formation between one of its outer carbon atoms and the neighboring hydrocarbon species. As can be seen in Table 4, at diamond (111)1 × 1, one of the outer C atoms of C_3H_2 bonds favorably to the neighboring hydrocarbon species. This results for diamond (111)1 × 1 in other ring structures than 6-rings.

The same line of thought can be made for the other species, explaining the different behavior at diamond (100)2 × 1 and diamond (111)1 × 1. For example, C_2H_2 is less successful in the formation of 6-rings at diamond (100)2 × 1 than at diamond (111)1 × 1. This can be explained by the fact that C_2H_2 is not forced to stand upright at diamond (100)2 × 1, resulting in a lower accessibility of the C atom that is the

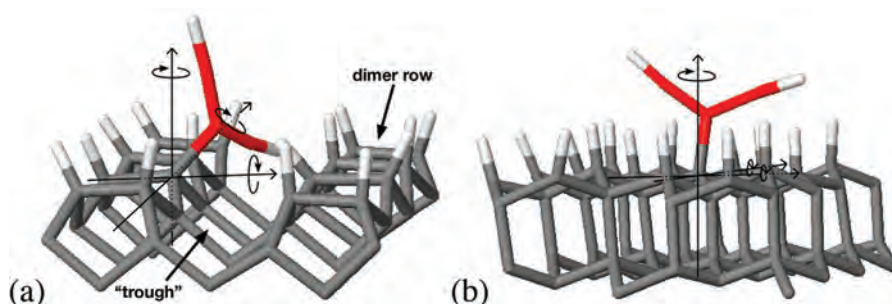


Figure 5. Local environment of a C_3H_2 radical at diamond $(100)2 \times 1$ (a) and diamond $(111)1 \times 1$ (b) surfaces. For clarity reasons, the structures are not shown in the ball and stick model but in the simple stick model. As in the other figures, gray, white, and red indicate carbon atoms, hydrogen atoms, and carbon adatoms, respectively. At diamond $(100)2 \times 1$, so-called “troughs” arise between the dimer chains, caused by the surface reconstruction. The x , y , and z rotation axes through the diamond surface atom to which the radical is stuck are shown. As can be seen, therefore, the sterical hindrance of the C_3H_2 species rotating about the x - and y -axis at the diamond $(100)2 \times 1$ surface is much smaller than that at the $(111)1 \times 1$ surface. This implicates that, for the diamond $(100)2 \times 1$ surface, it is more probable that a rotation about an axis at a small angle with the $\{x,y\}$ plane will be accepted than for the diamond $(111)1 \times 1$ surface.

farthest from the diamond surface. At diamond $(111)1 \times 1$, however, this C atom is within easy reach of the neighboring stuck hydrocarbon species, promoting the formation of 6-rings.

Summarizing, the structures of the diamond surfaces with their different topology, implying different sterical hindrance for trial rotations and displacements, seem to be an important contributor to the resulting structure: the higher the sterical hindrance at the diamond surface, the higher the probability that the structure remains in the configuration space of the minimum energy configuration and that it does not evolve into the minimum energy configuration. The energy difference between the starting and (converged) end configuration of the simulation is therefore a less determining contributor to the resulting structure.

Species Important for the Growth of NCD. For the hydrocarbon species that are important for NCD growth (see Table 1), the combinations that are the most likely to pursue the diamond structure have a probability of only ~ 0.3 (see Tables 5 and 6). These probabilities are much lower than those in the case of the species that are important for UNCD growth: Indeed, the combinations of species relevant for UNCD growth that are most likely to pursue the diamond structure have a probability of ~ 0.8 to form carbon 6-rings (see above). This difference can be explained by the fact that the species important for UNCD growth are less hydrogenated, implying less sterical hindrance at atoms having free electrons and therefore a higher reactivity.²³

For NCD, the probability of carbon 6-ring formation at the diamond $(100)2 \times 1$ surface is the highest for the combination of C_2H_2 with C_3H_2 (probability of 6-ring formation = 0.28, as shown in Table 5). For the diamond $(111)1 \times 1$ surface, it is the combination of C_2H_2 and CH_2 (probability of 6-ring formation = 0.30; see Table 6). Thus, the same observations as for the UNCD species can be made: The probabilities of 6-ring formation depend strongly on the surface and corresponding topology they are attached to. For diamond $(100)2 \times 1$, it appears that the hydrocarbon species containing more carbon atoms give rise to a greater probability to form a carbon 6-ring. For diamond $(111)1 \times 1$, it is the combination of CH_2 and C_2H_2 that will form the most carbon 6-rings. The carbon atoms that are involved in the formation of carbon 6-rings are the same as for the UNCD species. However, the combination of twice C_2H_2 at diamond $(100)2 \times 1$ (i.e., at the elevated temperature of

1100 K) will be able to form carbon 6-rings; the effect of the temperature is discussed below.

As in the case of UNCD, for diamond $(100)2 \times 1$, the 6-ring formation competes with the formation of other ring structures (7-rings). For CH_2 and C_2H_2 at diamond $(100)2 \times 1$, the competing resulting configuration is the formation of C_2H and CH_3 (see Table 5). Similar competing configurations resulting from hydrogen migration with formation of C_2H and C_xH_{y+1} are found for the different combinations of hydrocarbon species at diamond $(111)1 \times 1$ (see Table 6).

Effect of the Temperature. As shown in Table 1, two combinations of species at biradical sites are important for the growth of both UNCD and NCD: The combination of twice C_2H_2 and the combination of C_2H_2 and C_3H_2 . Those combinations were thus studied at 800 K as well as at 1100 K (accounting for growth conditions of UNCD and NCD, respectively). This enables us to investigate the effect of the temperatures on the growth of UNCD and NCD. In Tables 7–10, all configurations are shown that were formed at least once during the MMC simulations at the two diamond surfaces. As can be seen from the tables, the possible end configurations remain the same as the system temperature is raised (except for twice C_2H_2 at diamond $(100)2 \times 1$: At the higher temperature, carbon 6-rings are formed, in contrast to the case at the lower temperature). However, the probabilities of the final configurations change: The higher the temperature, the more the probabilities are spread out over the different possible resulting configurations. Therefore, the highest formation probability at the lower temperature decreases as the temperature is raised and the resulting configurations with the lowest probability become more probable at the higher temperature. This is a direct consequence of eq 5: The higher the temperature, the more probable become the populations of the higher energetic states. Note that the decrease of the potential energy differs for the lower and higher system temperatures. Since the energy difference cannot be related to an incomplete energy minimization (the convergence criterion is strict enough, see above), this difference must be related to local minima that are favorably populated at a certain temperature (i.e., local minima related to conformers).

No clear trend regarding the formation of carbon 6-rings can be drawn for the two temperatures: For the combination of twice C_2H_2 , the probability of 6-ring formation increases at diamond $(100)2 \times 1$ as the temperature is raised (from 0.00

Table 7. All Resulting Configurations from two C₂H₂ Species at a Biradical Site of Diamond (100)2 × 1^a

input configuration		resulting configuration			
C ₂ H ₂ and C ₂ H ₂ at diamond (100)2x1		new carbon 6-rings	new C-H bonds, no new C-C bonds	carbon 7-rings	no new bonds
800 K	Probability ΔE =	0.00	0.26 -3.98 eV	0.72 -5.03 eV	0.02 0.00 eV
1100 K	Probability ΔE =	0.16 -2.89 eV	0.38 -3.40 eV	0.44 -4.20 eV	0.02 0.00 eV

^aIn the left column, the input configuration is displayed. In the inner column, all possible resulting configurations from 50 MMC simulations are shown. The formation probabilities are shown for two different system temperatures, 800 K (typical for UNCD growth) and 1100 K (typical for NCD growth), together with the energy decrease. The energy decrease is calculated as the average energy decrease for the identical resulting configurations (the calculated standard error is smaller than 0.01). Identical structures are defined as structures with the same arrangement of chemical bonds. In the right column, the probability of energy minimization without the formation of new bonds can be found. Probabilities are calculated as relative occurrences of the given structures after the MMC simulation.

Table 8. All Resulting Configurations from Two C₂H₂ Species at a Biradical Site of Diamond (111)1 × 1^a

input configuration		resulting configuration			
C ₂ H ₂ and C ₂ H ₂ at diamond (111)1x1		new carbon 6-rings	new C-H bonds, no new C-C bonds	carbon 7-rings	no new bonds
800 K	Probability ΔE =	0.00	0.94 -3.41 eV	0.04 -4.68 eV	0.02 0.00 eV
1100 K	Probability ΔE =	0.00	0.88 -3.15 eV	0.08 -3.95 eV	0.04 0.00 eV

^aIn the left column, the input configuration is displayed. In the inner column, all possible resulting configurations from 50 MMC simulations are shown. The formation probabilities are shown for two different system temperatures, 800 K (typical for UNCD growth) and 1100 K (typical for NCD growth), together with the energy decrease. The energy decrease is calculated as the average energy decrease for the identical resulting configurations (the calculated standard error is smaller than 0.01). Identical structures are defined as structures with the same arrangement of chemical bonds. In the right column, the probability of energy minimization without the formation of new bonds can be found. Probabilities are calculated as relative occurrences of the given structures after the MMC simulation.

Table 9. All Resulting Configurations from C₂H₂ and C₃H₂ at a Biradical Site of Diamond (100)2 × 1^a

input configuration		resulting configuration			
C ₂ H ₂ and C ₃ H ₂ at diamond (100)2x1		new carbon 6-rings	new C-H bonds, no new C-C bonds	carbon 7-rings	no new bonds
800 K	Probability ΔE =	0.36 -5.10 eV	0.50 -3.71 eV	0.12 -5.20 eV	0.02 0.00 eV
1100 K	Probability ΔE =	0.28 -5.17 eV	0.32 -3.61 eV	0.38 -5.40 eV	0.02 0.00 eV

^aIn the left column, the input configuration is displayed. In the inner column, all possible resulting configurations from 50 MMC simulations are shown. The formation probabilities are shown for two different system temperatures, 800 K (typical for UNCD growth) and 1100 K (typical for NCD growth), together with the energy decrease. The energy decrease is calculated as the average energy decrease for the identical resulting configurations (the calculated standard error is smaller than 0.01). Identical structures are defined as structures with the same arrangement of chemical bonds. In the right column, the probability of energy minimization without the formation of new bonds can be found. Probabilities are calculated as relative occurrences of the given structures after the MMC simulation.

to 0.16; see Table 7), whereas the probability remains constant for diamond (111)1 × 1 (0.00; see Table 8). For the

combination of C₂H₂ and C₃H₂, the temperature has an opposite effect on the probability of 6-ring formation at

Table 10. All Resulting Configurations from C₂H₂ and C₃H₂ at a Biradical Site of Diamond (111)1 × 1^a

input configuration		resulting configuration			
C ₂ H ₂ and C ₃ H ₂ at diamond (111)1 × 1		new carbon 6-rings	new C–H bonds, no new C–C bonds	carbon 7-rings	no new bonds
800 K	Probability ΔE =	0.10 -5.95 eV	0.78 -4.31 eV	0.10 -5.79 eV	0.02 0.00 eV
1100 K	Probability ΔE =	0.18 -5.80 eV	0.60 -4.27 eV	0.20 -6.05 eV	0.02 0.00 eV

^aIn the left column, the input configuration is displayed. In the inner column, all possible resulting configurations from 50 MMC simulations are shown. The formation probabilities are shown for two different system temperatures, 800 K (typical for UNCD growth) and 1100 K (typical for NCD growth), together with the energy decrease. The energy decrease is calculated as the average energy decrease for the identical resulting configurations (the calculated standard error is smaller than 0.01). Identical structures are defined as structures with the same arrangement of chemical bonds. In the right column, the probability of energy minimization without the formation of new bonds can be found. Probabilities are calculated as relative occurrences of the given structures after the MMC simulation.

diamond (100)2 × 1 (decrease from 0.36 to 0.28; see Table 9) and (111)1 × 1 (increase from 0.10 to 0.18; see Table 10). Therefore, we can conclude that the temperature does not affect the relaxational events during diamond growth in a manner that it can explain the different growth regimes of UNCD and NCD. However, it is straightforward that the temperature can affect numerous other mechanisms that are important for diamond growth, e.g. sticking and etch events.²³

Conclusions

In this paper, we presented the results of a combined MD-MMC study of hydrocarbon species at flat diamond surfaces. The MD part of the code accounts for the simulation of impacting hydrocarbon species on diamond surfaces, and the MMC code simulates the slower relaxational events. This paper focuses on the relaxational behavior of hydrocarbon species at monoradical and biradical sites of diamond (100)2 × 1 and (111)1 × 1 surfaces.

The present implementation of the MMC algorithm enables the simulation of cluster rotation at the surfaces. It is shown that the implementation of rotation significantly reduces the number of MMC cycles that is needed to reach convergence in two of the three tested cases. This lowers the calculation time dramatically. In the other case, the number of MMC cycles does not decrease, which raises the calculation time (due to the calculation of trigonometric functions). However, the reduction of the high calculation time in the first two cases preponderates the increase of the rather short calculation time in the last case.

The species that are investigated are the ones that might affect the growth of UNCD and NCD; the selection is based on their concentrations close to the surface in combination with their sticking coefficients. When impacting monoradical sites at hydrogenated diamond (100)2 × 1 and (111)1 × 1 surfaces, no bonding changes are seen when applying the MMC algorithm, except for CH₂, which inserts into a surface dimer at diamond (100)2 × 1. The sequence of the bond breaking and formation as put forward by the MMC simulation mimics the mechanism, as proposed in the standard growth model of diamond. This justifies the application of our MD-MMC model for diamond growth.

Table 11. Summarizing Table of the Combinations of Hydrocarbon Species That Pursue the Diamond Structure the Most Efficiently, When Attached to Adjacent Radical Sites (i.e., those combinations have a high probability to form carbon 6-rings)^a

diamond surface	for UNCD	for NCD
(100)2 × 1	C ₃ and C ₃ H ₂ , C ₃ and C ₄ H ₂	C ₂ H ₂ and C ₃ H ₂
(111)1 × 1	C and C ₂ H ₂	CH ₂ and C ₂ H ₂

^aThe combinations of hydrocarbon species that are the most likely to pursue the diamond structure at typical NCD growth conditions have a probability of only ~0.3 to form carbon 6-rings (see text). These probabilities are much lower than in the case of species relevant for UNCD growth (~0.8), due to the fact that the species important for UNCD growth are less hydrogenated, implying less sterical hindrance at atoms having free electrons and therefore a higher reactivity.

In contrast to the behavior of hydrocarbon species at monoradical sites, the MMC simulations give rise to significant changes in the bonding structure when two hydrocarbon species are bound to two adjacent radical sites (i.e., the so-called “biradical sites”). This configuration of two hydrocarbon species at adjacent surfaces is indeed quite probable: Our MMC simulations of hydrocarbon species at monoradical sites have revealed that the bonding configuration as resulting from the MD simulations of impacting C_xH_y species is not altered by the MMC simulation (except for the case of CH₂, as mentioned above). Hence, it is well probable that if an impacting hydrocarbon species sticks to a dangling bond next to a previously stuck hydrocarbon species, the first hydrocarbon species still has one bond with the surface, regardless of the time between the two impacts, giving rise to two adjacent stuck hydrocarbon species.

In Table 11, the combinations of hydrocarbon species are listed that exhibit the greatest probability of carbon 6-ring formation when located on neighboring diamond surface atoms; those combinations contribute the most to the nucleation of new diamond layers. At diamond (100)2 × 1, hydrocarbon species containing more than one carbon atom are the most successful in pursuing the diamond structure. For diamond (111)1 × 1, the hydrocarbon species with one or two carbon atoms are the most important for the growth of (U)NCD. The different behaviors of the hydrocarbon species at the two diamond surfaces are due to the different surface structures: At diamond (100)2 × 1, the hydrocarbon species feel less sterical hindrance to rotate about axes at small angles

with the surface plane. This results in a better accessibility of atoms that can form bonds resulting in carbon 6-rings. At diamond (111)1 × 1, however, the hydrocarbon species are forced to stand upright, such that the smaller hydrocarbon species are more promoted to form carbon 6-rings. Hydrocarbon species at diamond (111)1 × 1 containing more than two carbon atoms will indeed form bonds by the carbon atoms that are the farthest from the surface, resulting in amorphous structures.

A few hydrocarbon species are relevant for the growth of both UNCD and NCD. This enabled us to investigate combinations of species at two different temperatures (800 and 1100 K, typical for the deposition of UNCD and NCD, respectively). We found that the temperature does not affect the relaxational events during diamond growth in a manner that can explain the different growth regimes of UNCD and NCD.

It has been shown that hydrocarbon species at diamond surfaces when attached to biradical sites contribute significantly to the growth of (U)NCD. Among the very reactive species, one can find C_xH_y species with $x \geq 2$. This should encourage the investigation of their behavior at a higher level of theory, in order to fill up the standard growth model.

Acknowledgment. M.E. is indebted to the Institute for the Promotion of Innovation through Science and Technology in Flanders (IWT—Vlaanderen) for financial support. E.N. acknowledges financial support from the Fund for Scientific Research—Flanders (FWO). This work was financially supported by the IAP-P6/42 project “Quantum Effects in Clusters and Nanowires” and the Fund for Scientific Research—Flanders (FWO). The calculation support of the core facility CALCUA, provided by the University of Antwerp, is gratefully acknowledged.

References

- Gruen, D. M. *Annu. Rev. Mater. Sci.* **1999**, *29*, 211–259.
- Philip, J.; Hess, P.; Feygelson, T.; Butler, J. E.; Chattopadhyay, S.; Chen, K. H.; Chen, L. C. *J. Appl. Phys.* **2003**, *93*, 2164–2171.
- Okrój, W.; Kamińska, M.; Klimek, L.; Szymański, W.; Walkowiak, B. *Diamond Relat. Mater.* **2006**, *15*, 1535–1539.
- Williams, O. A.; Daenen, M.; D’Haen, J.; Haenen, K.; Maes, J.; Moshchalkov, V. V.; Nesládek, M.; Gruen, D. M. *Diamond Relat. Mater.* **2006**, *15*, 654–658.
- Chu, P. K.; Li, L. *Mater. Chem. Phys.* **2006**, *96*, 253–277.
- Williams, O. A. *Semicond. Sci. Technol.* **2006**, *21*, R49–R56.
- Auciello, O.; Birrell, J.; Carlisle, J. A.; Gerbi, J. E.; Xiao, X. C.; Peng, B.; Espinosa, H. D. *J. Phys.: Condens. Matter* **2004**, *16*, R539–R552.
- May, P. W.; Mankelevich, Y. A. *J. Phys. Chem. C* **2008**, *112*, 12432–12441.
- May, P. W.; Harvey, J. N.; Smith, J. A.; Mankelevich, Y. A. *J. Appl. Phys.* **2006**, *99*, 104907.
- May, P. W.; Allan, N. L.; Ashfold, M. N. R.; Richley, J. C.; Mankelevich, Y. A. *J. Phys.: Condens. Matter* **2009**, *21*, 364203.
- Butler, J. E.; Mankelevich, Y. A.; Cheesman, A.; Ma, J.; Ashfold, M. N. R. *J. Phys.: Condens. Matter* **2009**, *21*, 364201.
- Netto, A.; Frenklach, M. *Diamond Relat. Mater.* **2005**, *14*, 1630–1646.
- Butler, J. E.; Oleynik, I. *Philos. Trans. R. Soc. London A* **2008**, *366*, 295–311.
- Skokov, S.; Weiner, B.; Frenklach, M. *J. Phys. Chem.* **1994**, *98*, 7073–7082.
- Ashfold, N. R.; May, P. W.; Petherbridge, J. R.; Rosser, K. N.; Smith, J. A.; Mankelevich, Y. A.; Suetin, N. V. *Phys. Chem. Chem. Phys.* **2001**, *3*, 3471–3485.
- Skokov, S.; Weiner, B.; Frenklach, M. *J. Phys. Chem.* **1994**, *98*, 8–11.
- Garrison, B. J.; Dawnkaski, E. J.; Srivastava, D.; Brenner, D. W. *Science* **1992**, *255*, 835–838.
- Agacino, E.; de la Mora, P. *Struct. Chem.* **2003**, *14*, 541–550.
- Kang, J. K.; Musgrave, C. B. *J. Chem. Phys.* **1958**, *17*, 7582–7587.
- Cheesman, A.; Harvey, J. N.; Ashfold, N. R. *J. Phys. Chem. A* **2008**, *112*, 11436–11448.
- Tamura, H.; Gordon, M. S. *Chem. Phys. Lett.* **2005**, *406*, 197–201.
- May, P. W. *Philos. Trans. R. Soc. London A* **2000**, *358*, 473–495.
- Eckert, M.; Neyts, E.; Bogaerts, A. *Chem. Vap. Deposition* **2008**, *14*, 213–223.
- D’Evelyn, M.; Graham, J.; Martin, L. *Diamond Relat. Mater.* **2001**, *10*, 1627–1632.
- Doll, J. D.; Voter, A. F. *Annu. Rev. Phys. Chem.* **1987**, *38*, 413–431.
- Voter, A. F.; Montalenti, F.; Germann, T. C. *Annu. Rev. Mater. Sci.* **2002**, *32*, 321–346.
- Barkema, G. T.; Mousseau, N. *Phys. Rev. Lett.* **1996**, *77*, 4358–4361.
- Sorensen, M. R.; Voter, A. F. *J. Chem. Phys.* **2000**, *112*, 9599–9606.
- Eckert, M.; Neyts, E.; Bogaerts, A. *CrystEngComm* **2009**, *11*, 1597–1608.
- Metropolis, N.; Rosenbluth, A. W.; Rosenbluth, M. N.; Teller, A. H.; Teller, E. *J. Chem. Phys.* **1953**, *21*, 1087–1092.
- Taguchi, M.; Hamaguchi, S. *Thin Solid Films* **2007**, *515*, 4879–4882.
- Ristein, J. *Appl. Phys. A: Mater. Sci. Process.* **2006**, *82*, 377–384.
- Garrison, B. J.; Kodali, P. B. S.; Srivastava, D. *Chem. Rev.* **1996**, *96*, 1327–1341.
- Zhu, W. J.; Pan, Z. Y.; Ho, Y. K.; Man, Z. Y. *Eur. Phys. J. D* **1999**, *5*, 83–88.
- Träskelin, P.; Salonen, E.; Nordlund, K.; Krasheninnikov, A. V.; Keinonen, J.; Wu, C. H. *J. Nucl. Mater.* **2003**, *313–316*, 52–55.
- Frenkel, D.; Smit, B. *Understanding Molecular Simulation*, 1st ed.; Academic Press: San Diego, 1996.
- Brenner, D. W. *Phys. Rev. B* **1990**, *42*, 9458–9471.
- Dyson, A. J.; Smith, P. V. *Surf. Sci.* **1994**, *316*, 309–316.
- Pastewka, L.; Pou, P.; Perez, R.; Gumbsch, P.; Moseler, M. *Phys. Rev. B* **2008**, *78*, 161402.
- Kaukonen, M.; Peräjoki, J.; Nieminen, R. M.; Jungnickel, G.; Frauenheim, T. *Phys. Rev. B: Condens. Matter Mater. Phys.* **2000**, *61*, 980–987.
- Liu, Y. H.; Neyts, E.; Bogaerts, A. *Diamond Relat. Mater.* **2006**, *15*, 1629–1635.
- Henkelman, G.; Jónsson, H. *Phys. Rev. Lett.* **2003**, *90*, 116101.
- Landau, D. P.; Binder, K. *A Guide to Monte Carlo Simulations in Statistical Physics*, 1st ed.; Cambridge University Press: Cambridge, 2000.
- Tamura, H.; Zhou, H.; Hirano, Y.; Takami, S.; Kubo, M.; Belosludov, R. V.; Miyamoto, A.; Imamura, A.; Gamo, M. N.; Ando, T. *Phys. Rev. B* **2000**, *62*, 16995–17003.